Journal of Power Sources 185 (2008) 790–800

Contents lists available at ScienceDirect

Journal of Power Sources

journal homepage: www.elsevier.com/locate/jpowsour

A study of solid oxide fuel cell stack failure by inducing abnormal behavior in a single cell test

Hyung-Tae Lim, Anil V. Virkar*

Department of Materials Science & Engineering, 122 South Central Campus Drive, Salt Lake City, UT 84112, United States

ARTICLE INFO

Article history:
Received 2 July 2008
Accepted 16 July 2008
Available online 29 July 2008

Keywords:
Solid oxide fuel cell
SOFC
Stack failure
Degradation

ABSTRACT

It is well known that cell imbalance can lead to failure of batteries. Prior theoretical modeling has shown that similar failure can occur in solid oxide fuel cell (SOFC) stacks due to cell imbalance. Central to failure model for SOFC stacks is the abnormal operation of a cell with cell voltage becoming negative. For investigation of SOFC stack failure by simulating abnormal behavior in a single cell test, thin yttria-stabilized zirconia (YSZ) electrolyte, anode-supported cells were tested at 800 °C with hydrogen as fuel and air as oxidant with and without an applied DC bias. When under a DC bias with cell operating under a negative voltage, rapid degradation occurred characterized by increased cell resistance. Visual and microscopic examination revealed that delamination occurred along the electrolyte/anode interface. The present results show that anode-supported SOFC stacks with YSZ electrolyte are prone to catastrophic failure due to internal pressure buildup, provided cell imbalance occurs. The present results also suggest that the greater the number of cells in an SOFC stack, the greater is the propensity to catastrophic failure.

1. Introduction

It has been known that cell imbalance characterized by higher resistance and lower capacity than the remaining cells in a series-connected battery can lead to failure of the entire battery [1–14]. During charging, voltage across such a cell behaving abnormally exceeds that across the other cells exhibiting normal behavior. Such a cell can overheat and result in cell failure which propagates to adjacent cells leading to the failure of the series leg. Failure of battery packs due to cell imbalance can also occur during discharge. There is extensive battery literature on premature failure due to cell imbalance, a problem which has defied a satisfactory solution. Many engineering solutions have been developed to minimize cell and battery failures. These include incorporating additional circuitry for charge equalization with capacitor/resistor banks, and independently monitoring individual cells [4–9,12–14]. Such an approach is possible if the number of cells in a battery is not too large. The greater the number of cells in series, the greater is the probability of cell imbalance. It is known that a battery having as few as 10 cells is subject to this problem and the occurrence of premature failure.

There is a significant parallel between batteries and fuel cells in that both are active electrochemical devices and a number of them must be connected in series to realize a sufficiently high voltage of practical value. In fuel cells, the problem is potentially more serious for two reasons: (1) The open circuit voltage (OCV) of a typical fuel cell is about 1 V, compared to 1.5 V for alkaline batteries or over 3 V for lithium ion batteries. Thus, to realize a given voltage, a greater number of fuel cells must be connected in series than typical batteries, which increases potential for imbalance. (2) For economic and practical reasons, current efforts are being directed towards increasing active area of fuel cells, in some cases, as large as 1000 cm^2 in size. The greater the cell active area, the greater is the potential for cell imbalance[1] and premature failure.

In a recent paper, one of the authors of this manuscript proposed a mechanism of failure in solid oxide fuel cell (SOFC) stacks due to cell imbalance [15]. The origin of failure lies in stack issues and yet depends on thermodynamics and transport theory [16–18]. All discussion in this paper is restricted to planar SOFC stacks. A survey of literature shows that no discussion of SOFC stack failures due to cell imbalance has been published (to the authors' knowledge) with the exception of the above-referenced recent paper [15]. Unpublished

* Corresponding author. Tel.: +1 801 581 5396; fax: +1 801 581 4816.
E-mail address: anil.virkar@m.cc.utah.edu (A.V. Virkar).

[1] In batteries, cell imbalance usually refers to differences in cell capacity and cell resistance. In fuel cells, cell imbalance would mean primarily differences in cell resistance and possible differences in channel dimensions restricting gas flow, which would be analogous to battery cells having different capacities.

0378-7753/$ – see front matter © 2008 Elsevier B.V. All rights reserved.
doi:10.1016/j.jpowsour.2008.07.051

Nomenclature

A_{del}	Fraction of interface area delaminated
e	electronic charge (C)
E	Nernst voltage (V)
E_b	DC bias voltage
$E_s = (N-1)E$	source voltage (open circuit voltage of $(N-1)$ series-connected identical cells)
F	Faraday constant ($C\,mol^{-1}$)
I_i	ionic current density through the cell ($A\,cm^{-2}$)
I_e	electronic current density through the cell ($A\,cm^{-2}$)
I_L	load current
k_B	Boltzmann constant
N	number of cells in a stack
p_{O_2}	oxygen partial pressure
$p_{O_2}^{amb}$	oxygen pressure in the atmosphere (0.21 atm)
$p_{O_2}^{int}$	oxygen pressure at the interface
r_i^c	area specific cathode/electrolyte interface ionic resistance (Ωcm^2)
r_i^a	area specific anode/electrolyte interface ionic resistance (Ωcm^2)
r_i^{el}	area specific electrolyte ionic resistance (Ωcm^2)
r_e^c	area specific cathode/electrolyte interface electronic resistance (Ωcm^2)
r_e^a	area specific anode/electrolyte interface electronic resistance (Ωcm^2)
r_e^{el}	area specific electrolyte electronic resistance (Ωcm^2)
R	ideal gas constant
$R_i = r_i^c + r_i^{el} + r_i^a$	area specific ionic cell resistance (Ωcm^2)
$R_e = r_e^c + r_e^{el} + r_e^a$	area specific electronic cell resistance (Ωcm^2)
R_L	load resistance
$R_s = (N-1)R_C$	source resistance (resistance of $(N-1)$ series-connected identical cells)
T	temperature (K)
V_C	cell voltage (V)

Greek letters

Φ	electrostatic potential
$\varphi = -\frac{\tilde{\mu}_e}{e}$	reduced (negative) electrochemical potential of electrons or electric potential (V)
φ^I	electric potential of the cathode (V)
φ^{II}	electric potential of the anode (V)
$\tilde{\mu}_e$	electrochemical potential of electrons
μ_e	chemical potential of electrons
μ_{O_2}	chemical potential of oxygen
$\mu_{O_2}^{cathode} = \mu_{O_2}^{I}$	chemical potential of oxygen in the gas phase at the cathode (just outside the electrolyte/cathode interface in the cathode)
$\mu_{O_2}^{anode} = \mu_{O_2}^{II}$	chemical potential of oxygen in the gas phase at the anode (just outside the electrolyte/anode interface in the anode)
$\mu_{O_2}^{electrolyte}$	chemical potential of oxygen within the electrolyte
$\mu_{O_2}^{c}$	chemical potential of oxygen in the electrolyte, just under the cathode
$\mu_{O_2}^{a}$	chemical potential of oxygen in the electrolyte, just under the anode

work has shown that stack failures do occur even when a single cell in an otherwise normal stack exhibits abnormal behavior (high resistance).

One of the authors of this paper has proposed a model describing failure of cationic and anionic conducting solid electrolytes in such devices as batteries and electrochemically driven oxygen separation systems [19,20]. Subsequent work showed that electrically driven system is fundamentally different in minute (albeit important) details than a device such as a single SOFC [21]. It was shown that chemical potential of a neutral species (e.g. oxygen, O_2) inside an electrolyte of a single SOFC is mathematically bounded by corresponding values in the gas phases at the electrodes, $\mu_{O_2}^{anode}$ and $\mu_{O_2}^{cathode}$. That is, the chemical potential of oxygen, μ_{O_2} in the solid electrolyte of a single SOFC is bounded by $\mu_{O_2}^{anode}$ and $\mu_{O_2}^{cathode}$; or $\mu_{O_2}^{anode} \leq \mu_{O_2}^{electrolyte} \leq \mu_{O_2}^{cathode}$ [21]. Local equilibrium[2] implies that μ_{O_2} (as a gas) is completely and uniquely defined (consistent with 'local' conditions) in a fully dense electrolyte, and assuming ideal gas law it means $\mu_{O_2} = \mu_{O_2}^{o} + k_B T \ln p_{O_2}$[3] is valid inside a fully dense solid [16–18]. Thus the μ_{O_2} and p_{O_2} in a fully dense solid electrolyte are meaningfully defined. This is well known in the established transport theory, although its significance and implications are rarely emphasized [17,18].

The analysis shows that in electrically driven systems (such as oxygen separation under applied voltage), μ_{O_2} in the solid electrolyte need not be mathematically bounded by corresponding values in the gas phases [21]. That is, the analysis shows that $\mu_{O_2}^{anode} >=< \mu_{O_2}^{electrolyte}$ and $\mu_{O_2}^{electrolyte} >=< \mu_{O_2}^{cathode}$ or the $\mu_{O_2}^{electrolyte}$ can lie outside the cathode–anode range [21]. If the $\mu_{O_2}^{electrolyte}$ is too low, local electrolyte decomposition may occur by a reaction of the type $ZrO_2 \rightarrow Zr + O_2$. If the $\mu_{O_2}^{electrolyte}$ is too large, high internal μ_{O_2} may lead to cracking. It can be shown that oxygen gas can 'precipitate' at defects (may be small pores, grain boundaries, etc.) and force the solid open – that is force it to crack [20]. Various transport parameters (electrolyte and interface) determine if $\mu_{O_2}^{electrolyte}$ falls below the decomposition potential or increases to a value high enough to generate locally high internal pressures and cause cracking and failure [15,21]. The general conclusions of the work show that whether the μ_{O_2} is bounded or not depends on the relative directions of ionic and electronic currents through the electrolyte – if ionic and electronic currents through the electrolyte are in opposite directions, μ_{O_2} is bounded; if ionic and electronic currents through the electrolyte are in the same direction, μ_{O_2} need not be bounded [21]. The magnitude of the electronic current may be very small compared to ionic current, but still its direction is important and can have a profound effect on membrane stability [21].

1.1. An SOFC stack

If all cells (repeat units) in a stack have the same resistance, behavior of each cell in the stack is the same as an isolated (single) SOFC or a repeat unit. However, if one (or more) cells exhibit higher resistance than the rest, such a cell can be electrically driven. An extreme case consists of a bad cell (one with a higher resistance) being driven by the rest of the cells such that voltage across the driven cell becomes negative. This is illustrated via the following example. Consider a stack with 100 cells. Let us suppose 99 of them

[2] I. Prigogine's Nobel lecture (1977), www.nobelprize.org.

[3] If the μ_{O_2} is defined on a per mole basis, the Boltzmann constant, k_B, is replaced by the gas constant, R.

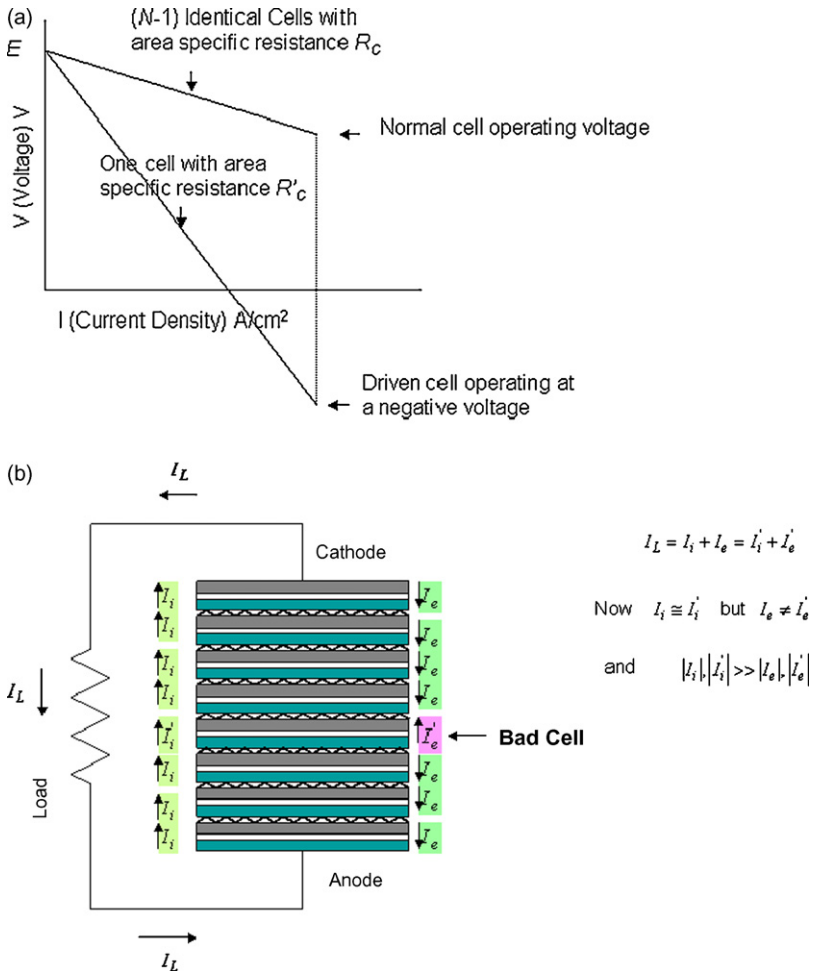

Fig. 1. (a) Voltage per cell vs. current density in an SOFC stack with a total of N cells. Of the cells, $(N-1)$ are all identical with ASR = R_C, and one cell has a higher ASR, R'_C, namely $R'_C > R_C$. (b) An SOFC stack with $(N-1)$ identical cells and one cell having a higher resistance and operating under a negative voltage. The predominant current through each cell is ionic, with the electronic current through the cell being negligible. In the cell operating under a negative voltage, the ionic and the electronic currents are in the same direction.

are identical with an area specific resistance (ASR) of each being 0.5 Ωcm^2. However, there is one bad cell with an ASR of 1.5 Ωcm^2. If the OCV is 1 V, and 99 cells are operated at 0.6 V, the current density is 0.8 A cm^{-2}. Since all cells are connected in series, current through the bad cell is also 0.8 A cm^{-2}. As the ASR of the bad cell is 1.5 Ωcm^2, voltage drop across this cell is 1.2 V. But the OCV for each cell is 1 V. Thus, voltage across the bad cell is given by $1 - 1.2 = -0.2$ V; that is, bad cell operating under a negative voltage. Fig. 1(a) shows a schematic of such a situation.

1.2. Directions of ionic and electronic currents and chemical potentials

In terms of ionic current density, I_i, through the electrolyte, electronic current density, I_e, *through* the electrolyte (however small), μ_{O_2} *in the electrolyte* just inside cathode ($\mu^c_{O_2}$) and just inside anode ($\mu^a_{O_2}$) are given by ref. [21][4]

$$\mu^c_{O_2} = \mu^I_{O_2} + 4e(r^c_i I_i - r^c_e I_e) \quad (1)$$

$$\mu^a_{O_2} = \mu^{II}_{O_2} - 4e(r^a_i I_i - r^a_e I_e) \quad (2)$$

where $\mu^I_{O_2} = \mu^{cathode}_{O_2}$ is the μ_{O_2} in the cathode gas, $\mu^{II}_{O_2} = \mu^{anode}_{O_2}$ is the μ_{O_2} in the anode gas, r^c_i is the ionic interfacial area specific resistance at the cathode/electrolyte interface, r^c_e is the electronic interfacial area specific resistance at the cathode/electrolyte interface, r^a_i is the ionic interfacial area specific resistance at the anode/electrolyte interface, and r^a_e is the electronic interfacial area specific resistance at the anode/electrolyte interface [15,21]. The oxygen ion flux through the electrolyte occurs from the cathode to the anode. Thus, ionic current density $I_i < 0$[5]. When a cell is operating normally, cathode is at a higher electric potential, φ (where $\varphi = -\tilde{\mu}_e/e$ and $\tilde{\mu}_e = \mu_e - e\Phi$ is the electrochemical potential of electrons, μ_e is the chemical potential of electrons, e is electronic charge, and Φ is electrostatic potential) than the anode. Thus, electron flux *through* electrolyte, however small, occurs from anode to cathode. Thus, electronic current density $I_e > 0$. That is, I_i and I_e are of opposite signs. Then, Eqs. (1) and (2) become [15,21]

$$\mu^c_{O_2} = \mu^I_{O_2} + 4e(r^c_i I_i - r^c_e I_e) = \mu^I_{O_2} - 4e(r^c_i |I_i| + r^c_e |I_e|) < \mu^I_{O_2} \quad (3)$$

[4] The μ_e, $\tilde{\mu}_e$, and μ_{O_2} are defined here on a per molecule basis. If defined on a per mole basis, the electronic charge, e, is replaced by the Faraday constant, F.

[5] The positive 'x' direction is taken to be from the cathode (through the electrolyte) to the anode. Thus, oxygen ions transport along the positive 'x' direction, which constitutes a negative ionic current since oxygen ions are negatively charged.

and

$$\mu^{a}_{O_2} = \mu^{II}_{O_2} - 4e(r^{a}_{i} I_i - r^{a}_{e} I_e) = \mu^{II}_{O_2} + 4e(r^{a}_{i} |I_i| + r^{a}_{e} |I_e|) > \mu^{II}_{O_2} \quad (4)$$

This means, $\mu^{I}_{O_2} \geq \mu^{c}_{O_2} > \mu^{a}_{O_2} \geq \mu^{II}_{O_2}$ [15,21]. That is, when a cell is operating properly (normally), μ_{O_2} within the electrolyte is mathematically bounded by corresponding values at the two electrodes (gas phases).

For the illustration with 100 cells, this means 99 cells are operating normally (the cathode at a higher electric potential, φ^{I}, than the anode, φ^{II}, or $\varphi^{I} - \varphi^{II} > 0$) but one cell is operating abnormally (the anode at a higher electric potential, $\varphi^{II'}$, than the cathode, $\varphi^{I'}$, or $\varphi^{II'} - \varphi^{I'} > 0$). For the cell operating abnormally (negative terminal voltage, anode at a higher electric potential than cathode), note that the direction of ionic current is the same as the rest of the cells but that of electronic current has reversed (Fig. 1(b)). In this cell, electron flow *through* the electrolyte also occurs from the cathode to the anode. Thus, for this cell, $I'_i < 0$ and $I'_e < 0$. Then Eqs. (1) and (2) become [15,21]

$$\mu^{c'}_{O_2} = \mu^{I}_{O_2} + 4e(r^{c'}_{i} I'_i - r^{c'}_{e} I'_e) = \mu^{I}_{O_2} - 4e(r^{c'}_{i} |I'_i| - r^{c'}_{e} |I'_e|) \quad (5)$$

and

$$\mu^{a'}_{O_2} = \mu^{II}_{O_2} - 4e(r^{a'}_{i} I'_i - r^{a'}_{e} I'_e) = \mu^{II}_{O_2} + 4e(r^{a'}_{i} |I'_i| - r^{a'}_{e} |I'_e|) \quad (6)$$

In Eqs. (5) and (6), various parameters are given with a 'prime', namely, $r^{c'}_{i}$, $r^{c'}_{e}$, $r^{a'}_{i}$, $r^{a'}_{e}$, $\varphi^{II'}$, $\varphi^{I'}$, $\mu^{a'}_{O_2}$, and $\mu^{c'}_{O_2}$ to emphasize a cell behaving abnormally. A key point is that the magnitude of electronic current is negligible compared to ionic current through all cells, including the cell behaving abnormally. Note that

$$I_i + I_e = I'_i + I'_e = I_L \quad (7)$$

where I_L is the load current[6] measured in the external circuit. As the electrolyte is an ionic conductor, $|I_i|, |I'_i| >> |I_e|, |I'_e|$, and thus $I_i \cong I'_i$ but $I_e \neq I'_e$. Important difference between cells behaving normally and those behaving abnormally is the difference in the signs of I_e and I'_e (Fig. 1(b)). The relative magnitudes of $r^{c'}_{i} |I'_i|$ and $r^{c'}_{e} |I'_e|$ determine whether $\mu^{c'}_{O_2}$ is greater or smaller than $\mu^{I}_{O_2}$ (Eq. (5)), and relative magnitudes of $r^{a'}_{i} |I'_i|$ and $r^{a'}_{e} |I'_e|$ determine whether $\mu^{a'}_{O_2}$ is greater or smaller than $\mu^{II}_{O_2}$ (Eq. (6)). Such a cell can degrade, and degradation may propagate to adjacent cells. This is the fundamental mechanism of SOFC stack degradation proposed previously [15].

In ref. [15], cathode activity was assumed to be excellent, that is $r^{c'}_{i} \approx 0$ such that $r^{c'}_{e} |I'_e| >> r^{c'}_{i} |I'_i|$. For this case, $\mu^{c'}_{O_2} \approx \mu^{I}_{O_2} + 4er^{c'}_{e} |I'_e| > \mu^{I}_{O_2}$ during abnormal cell behavior. Should this situation occur, cell degradation will manifest as cathode delamination. There are, however, many possibilities depending upon relative values of transport parameters [15,21]. For example, if $r^{a'}_{i} |I'_i| >> r^{a'}_{e} |I'_e|$ and $r^{c'}_{i} |I'_i| >> r^{c'}_{e} |I'_e|$, then $\mu^{a'}_{O_2} > \mu^{II}_{O_2}$ and $\mu^{c'}_{O_2} < \mu^{I}_{O_2}$. Then delamination may occur at anode/electrolyte interface. The objective of this work is to experimentally determine if delamination occurs under abnormal behavior and the location of delamination.

1.3. SOFC stack with one cell having a higher resistance than the rest of the cells

We consider an SOFC stack with N cells of which $(N-1)$ cells each has resistance R_C, and one (bad) cell has resistance R'_C such that $R'_C > R_C$. The Nernst voltage for each cell (including the bad cell) is E. A simplified equivalent circuit (neglecting low level parallel electronic current [15,21]) is given in Fig. 2(a). The net current is given by

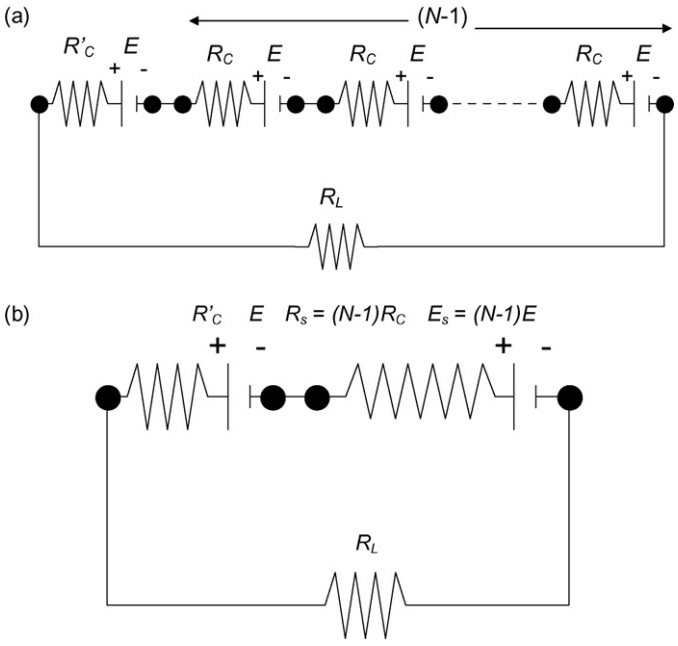

Fig. 2. (a) A simplified equivalent circuit for an SOFC stack. $(N-1)$ cells are identical with resistance R_C. One cell has a resistance R'_C where $R'_C > R_C$. The Nernst voltages are the same for all cells. R_L is the external load. (b) An equivalent circuit for the same stack. The $(N-1)$ identical cells are lumped as $E_s = (N-1)E$ and $R_s = (N-1)R_C$.

$$I_L = \frac{NE}{(N-1)R_C + R'_C + R_L} \quad (8)$$

where R_L is the load. Fig. 1 is a schematic of a SOFC stack. Equivalent circuit by lumping $(N-1)$ identical cells into one source is given in Fig. 2(b) with $E_s = (N-1)E$ and $R_s = (N-1)R_C$.

1.4. Simulation of abnormal cell behavior in a stack by a single cell test

Central to the mechanism of SOFC stack failure model proposed in ref. [15] is the operation of at least one cell under a negative voltage. In a stack containing many cells, this can occur as some changes in cell and repeat unit characteristics occur during operation, and without the experimenter/operator's knowledge unless voltages on individual cells are monitored. This suggests that stack failure model can be verified on a single cell, provided it is operated under a negative voltage (anode at a higher electric potential than cathode). Experimental arrangement consists of externally connecting a variable DC power supply to a cell, in addition to load, such that the positive of the power supply is connected to the anode and negative of the power supply is connected to the cathode. The corresponding equivalent circuit is shown in Fig. 3(a) (compare this to equivalent circuit for SOFC stack in Fig. 2(b)). If the externally applied voltage from the DC power supply is E_b (which would be like E_s for an actual SOFC stack) and if load is R_L (which for SOFC stack is the sum of R_s and load), voltage across the cell is given by

$$V_C = E - IR'_C = E - \left(\frac{E + E_b}{R'_C + R_L}\right) R'_C = \frac{ER_L - E_b R'_C}{R'_C + R_L} \quad (9)$$

If $E_b R'_C < ER_L$, $V_C > 0$, and the cell behaves normally. However, if $E_b R'_C > ER_L$, cell voltage will be negative, that is, $V_C < 0$, which replicates abnormal cell behavior in an SOFC stack. Fig. 3(b) shows

[6] As i_i and i_e are current densities (A cm^{-2}) through the electrolyte, I_L is the load current defined per unit electrolyte/electrode interface area (A cm^{-2}).

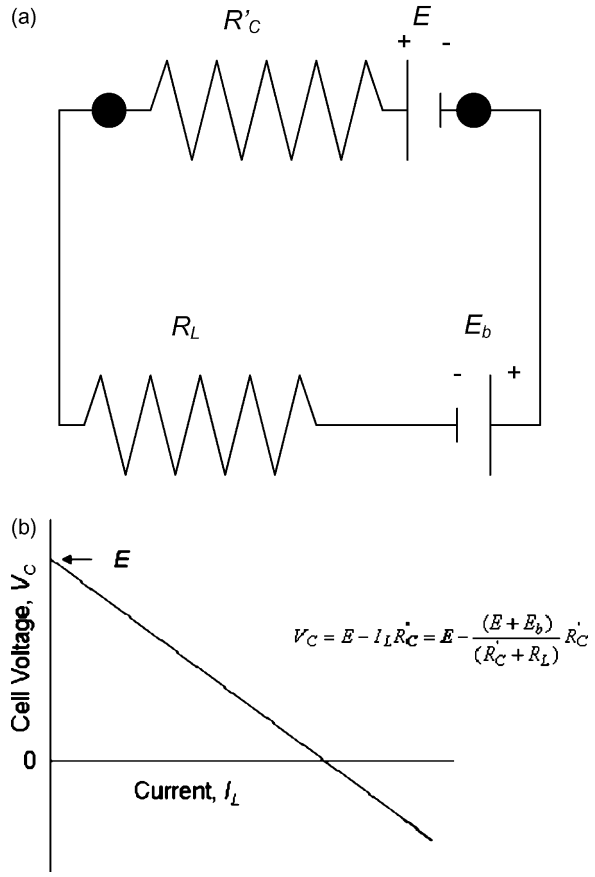

Fig. 3. (a) An equivalent circuit for simulating a bad cell behavior in an SOFC stack using a single cell test. E_b is external bias and R_L is the load. (b) A schematic of the voltage vs. current plot for the test procedure shown in (a). As the E_b is increased, the cell is forced to operate under a negative voltage.

anticipated voltage vs. current plot as E_b is varied. The objective of this work is to simulate such a situation using a single cell test. The experimental procedure and results obtained are presented and discussed in what follows.

2. Experimental procedure

2.1. Demonstration of abnormal behavior in an alkaline cell battery

The objective of this experiment was to demonstrate operation of an off-the-shelf alkaline cell under a negative voltage in a battery. In order to simulate this situation, an experiment was conducted on standard alkaline cells of sizes D and AAA. Their voltage vs. current characteristics were measured. D and AAA cells have different sizes, which results in different cell resistances (and capacities). Their chemistries are the same, and thus exhibit the same OCV. Eight D cells and one AAA cell were connected in series. The voltage vs. current characteristics of the assembled battery (placed in a hood) was recorded. The voltage across the AAA cell was also recorded. As all cells were connected in series, for any one measurement, current through each cell was the same.

2.2. Solid oxide fuel cell fabrication

A typical solid oxide fuel cell used in this work was anode-supported comprising six distinct layers as shown in Fig. 4. Cells were fabricated using the following procedure. Anode support

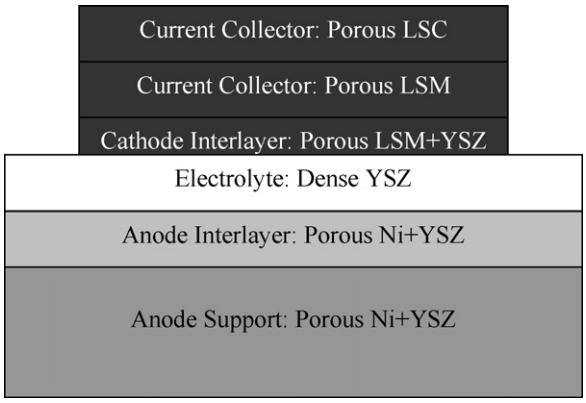

Fig. 4. A schematic of anode-supported cells comprising six layers used in this work.

tape containing 65 wt.% NiO and 35 wt.% yttria-stabilized zirconia (YSZ) (composition: 8 mol.% Y_2O_3 and 92 mol.% ZrO_2), anode functional layer tape containing 60 wt.% NiO and 40 wt.% YSZ and YSZ electrolyte layer tape were prepared. These three tapes were laminated into one tape. The laminated tape was punched into discs of 3.7 cm diameter, bisque-fired at 950 °C for 2 h, and sintered at 1400 °C for 2 h. The thickness of the electrolyte was ~10 μm. Porous cathode functional layer containing 50 wt.% LSM and 50 wt.% YSZ was screen-printed on the electrolyte surface followed by firing at 1185 °C. A layer of porous LSM was applied over the cathode functional layer followed by firing at 1165 °C. Finally, a layer of porous LSC was applied followed by firing at 1100 °C.

2.3. SOFC degradation testing by applying an external DC bias

A cell was spring loaded in a specially designed fixture with a mica gasket at the fuel side. All measurements were made at a cell temperature of 800 °C. A gas mixture with 10% H_2 and balance nitrogen was circulated over the anode surface to reduce NiO to Ni. Fuel was then changed to ~100% H_2 for cell tests while air was circulated past the cathode. The following two types of tests were performed. (1) Cell voltage and current density under fixed external load were measured without applying a DC bias ($E_b = 0$). After cell voltage under load stabilized, a DC bias was applied ($E_b > 0$) using a power supply to operate the cell under a negative voltage ($V_C < 0$) (Fig. 3(a)). The cell was operated in a constant current mode. As the cell resistance changed due to degradation, applied DC bias automatically adjusted to maintain current constant. This simulates abnormal cell behavior in an SOFC stack. This procedure was repeated one more time, and the test was discontinued. (2) Performance characteristics were measured on another cell without applying a DC bias. The external load was removed, and OCV was measured. Then a DC bias was applied and the cell was operated under a negative voltage in a constant current mode. After some time, external bias and load were removed. The OCV and cell performance characteristics were again measured. Then external DC bias was applied and cell was again operated under a negative voltage in a constant current mode. After some time, external bias was removed and cell performance was measured. After each test under a negative voltage, any increase in cell ASR could be attributed to damage created during cell operation under a negative voltage. Test procedure is illustrated in Fig. 5.

2.4. Post test examination

After testing, cells were observed visually. Cells were also fractured and possible damage was examined visually and by scanning electron microscopy (SEM).

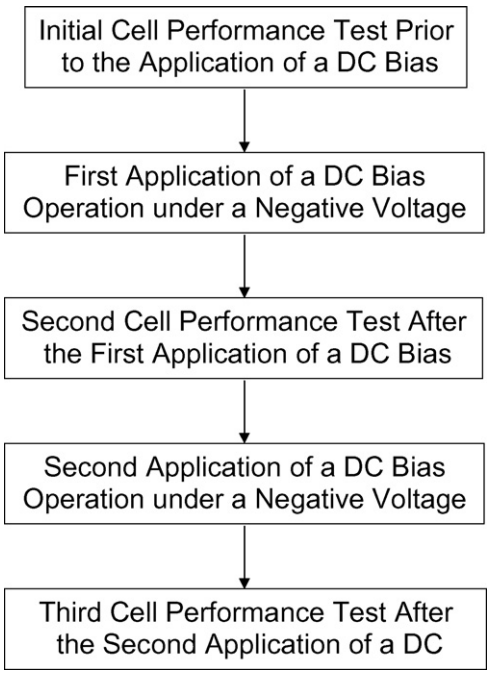

Fig. 5. The protocol used for cell testing under a negative voltage.

2.5. Generation and measurement of high internal oxygen pressures

To electrochemically generate and measure internal p_{O_2} under an applied voltage, the following experiment was performed. A bi-layer sample of YSZ and YSZ + ceria was fabricated. Some ceria was added to increase electronic conductivity in part of the sample

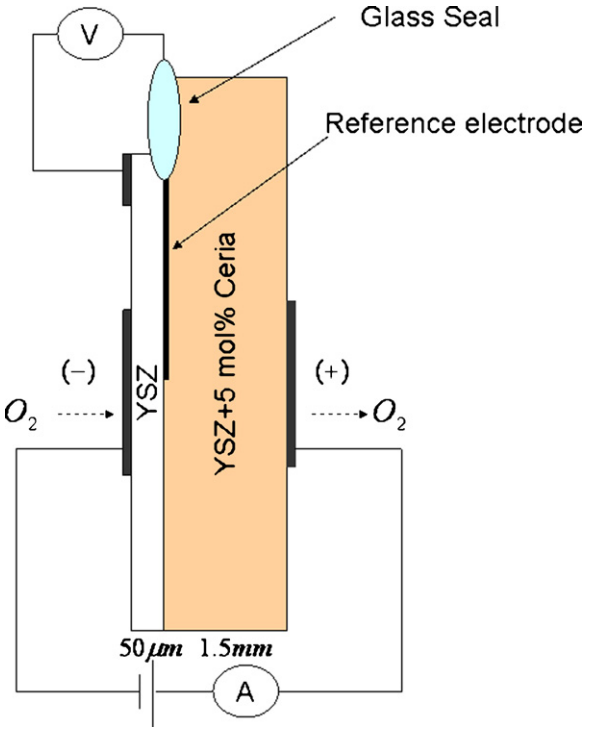

Fig. 6. A schematic of the YSZ/YSZ + ceria bi-layer cell and test procedure. A reference electrode is embedded at the interface and is isolated from the atmosphere using an oxygen impermeable sealing glass.

[20]. The following procedure was used.Sample fabrication: A powder mixture with 95 mol.% 8YSZ and 5 mol.% cerium oxide was ball milled for 24 hrs. A disc of 3.3 cm in diameter and 2 mm in thickness was pressed and bisque-fired at 950 °C. Platinum paste was applied as a thin and a narrow strip on one face of the disk. A slurry of 8YSZ was prepared in butyl alcohol. The YSZ slurry was drop-coated over most of the disk surface with the platinum strip except for a small part of the Pt strip. The bi-layer cell was sintered at 1450 °C for 4 hrs. The YSZ layer thickness was 50 μm. The YSZ + ceria layer was ground down to ∼1.5 mm from the other side. Platinum paste was applied as electrodes on the two surfaces of the disk. A thin layer of platinum as a reference electrode was also applied on the YSZ layer for measuring voltage between this (exposed) electrode and the embedded electrode positioned at YSZ/YSZ + ceria interface. Platinum wires were attached to all electrodes. Exposed part of the embedded reference electrode was coated with a paste of an oxygen impermeable sealing glass in ethylene glycol, and fired at 850 °C to isolate it from the atmosphere [22].Cell test: The bi-layer disk was loaded in a test fixture and inserted into a tube furnace. A voltmeter was connected between the surface and embedded reference electrodes. The disk was heated to 800 °C in air. A DC voltage (1 V) was applied across the cell, with the YSZ side electrode functioning as cathode and the YSZ + ceria side electrode as anode. That is, oxygen was pumped through the cell from cathode to anode. Voltage between the two reference electrodes was continuously monitored. Fig. 6 shows a schematic of the bi-layer sample and test procedure.

3. Results and discussion

3.1. Demonstration of abnormal behavior in an alkaline cell battery

Voltage–current behaviors for D and AAA cells were measured. The OCV for each cell was ∼1.55 V. The resistances of D and AAA cells were 0.267 Ω and 0.453 Ω, respectively. Fig. 7(a) shows results of a battery test in which eight D cells and one AAA cell were connected in series. Upper trace is for the complete battery. The OCV was ∼14.2 V and the battery resistance was ∼2.275 Ω. The lower trace is for the AAA cell in the battery. At a current of ∼2.9 A, the battery voltage was ∼8.2 V. The corresponding voltage across the AAA cell was ∼0 V. Beyond 2.9 A, the AAA cell operated under a negative voltage. The voltage on this cell also continued to decrease (increase in magnitude) at constant current once voltage was negative (Fig. 7(b)). This represents abnormal behavior for the cell operating under a negative voltage and results from a significantly greater resistance than the D cells. The maximum current passed through the battery was 4.5 A. The corresponding voltage across the battery was ∼5.0 V, that across each D cell was ∼0.645 V and that across the AAA cell was −0.4 V, which kept decreasing (increasing in magnitude). The test demonstrated that a cell with a higher resistance than the remaining cells in a battery could be operated under a negative voltage and continued to degrade. This constitutes abnormal behavior. The main objective of this work is to examine the role of abnormal cell behavior in an SOFC stack and its implications concerning stack failure.

3.2. Solid oxide fuel cell (SOFC) tests without and with an applied DC bias

Fig. 8 shows results of an SOFC test under no applied bias. The OCV was ∼1.04 V. Once the cell stabilized an external load was connected and the cell was operated under a constant current ($I_L = 0.82\,A\,cm^{-2}$) for ∼360 min (6 h). The voltage initially varied from ∼0.6 V to ∼0.645 V for an hour, indicating a

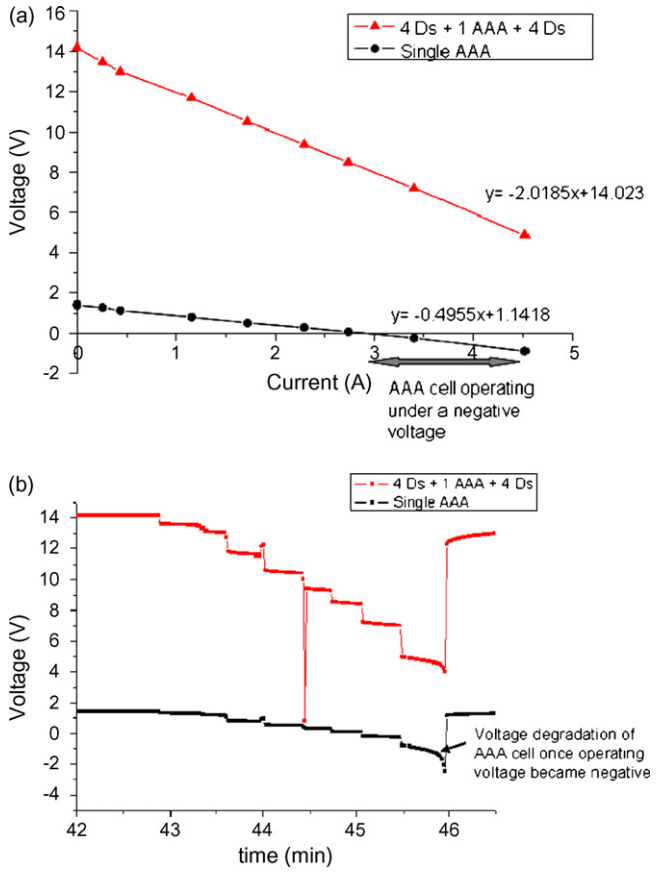

Fig. 7. (a) Voltage vs. current performance test on a battery with eight D cells and one AAA cell in series. For current >2.9 A, the AAA cell operated under a negative voltage – that is behaving abnormally. (b) Voltage vs. time across the eight D cells + one AAA cell battery and across the AAA cell as the external load was varied. Once the voltage across the AAA cell became negative, the cell began to degrade.

slight improvement in performance. Thereafter, voltage remained constant, indicating stable cell performance. The cell ASR was $R_C \approx 0.482\,\Omega\text{cm}^2$. A DC bias $E_b \approx 2$ V was then applied as shown in Fig. 3(a). The corresponding cell voltage was −0.142 V (anode at a higher voltage than cathode – cell operation under a negative voltage). The test was conducted under constant current ($I_L = 2.14\,\text{A cm}^{-2}$). The cell voltage continually decreased (increase in magnitude), similar to imbalance in alkaline cell tests (Fig. 7(b)).

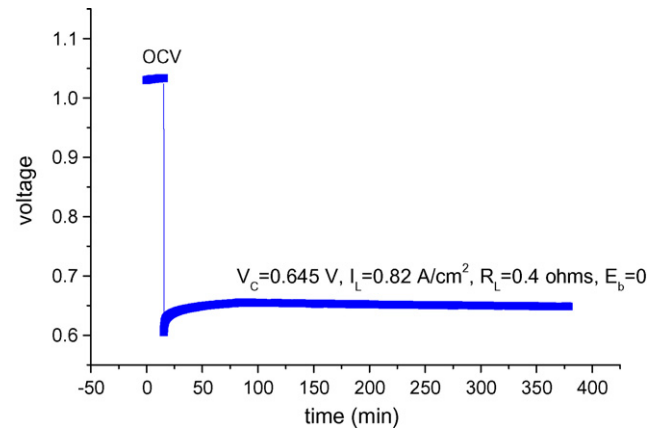

Fig. 8. A single SOFC test at 800 °C with hydrogen as fuel and air as oxidant. Stable performance over the duration of the test (~6 h).

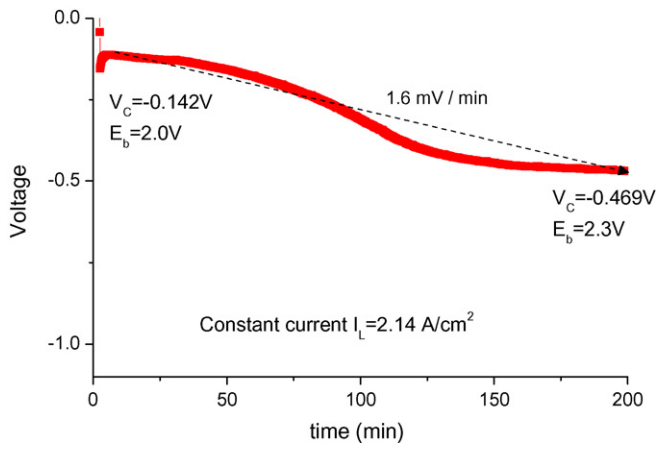

Fig. 9. Operation of the cell under an applied DC bias with cell operating under a negative voltage and in a constant current mode (current density = 2.14 A cm^{-2}). Over the duration of test (~200 min), cell voltage decreased from −0.142 V to −0.469 V.

After about 200 min, the V_C dropped to −0.469 V at an approximate rate of −1.6 mV min^{-1} and to maintain current constant, E_b automatically increased to ~2.3 V (Fig. 9). The bias was removed and the cell was maintained under open circuit condition for a period of time. Again a DC bias was applied and the cell was operated at $I_L = 2.17\,\text{A cm}^{-2}$ for about 10 min. The V_C initially was −0.77 V and decreased to −1.0 V at a rate of −23 mV min^{-1} (Fig. 10). The corresponding E_b varied between 3.2 V and 3.3 V. The lower initial voltage (higher magnitude) at the beginning of the second test (−0.77 V) compared to that at the end of the first test (−0.469 V) indicated that cell resistance continued to increase after the end of first test even when idling. That is, damage induced during the first test continued to propagate even when idled. The cell was cooled to room temperature and examined visually. It was observed that the cell had delaminated. The cross section of the delaminated cell was examined in an SEM. Fig. 11(a) shows that the YSZ electrolyte layer was bonded to the cathode but had completely delaminated from the anode. Another cell was subjected to a similar test. The cell was removed in a partially delaminated state. Fig. 11(b) shows that in this case also, delamination occurred along (actually close to) the electrolyte/anode interface (just inside the electrolyte).

The observations just described have important implications. First, this means high p_{O_2} in the electrolyte *just* under anode/electrolyte interface must have formed when operated

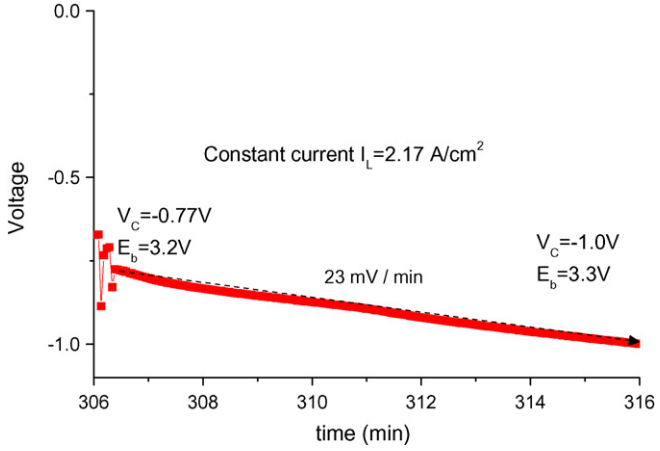

Fig. 10. Another test at a constant current of 2.17 A cm^{-2} under an applied DC bias on the same cell as in Fig. 9. The cell voltage varied between −0.77 V and −1.0 V.

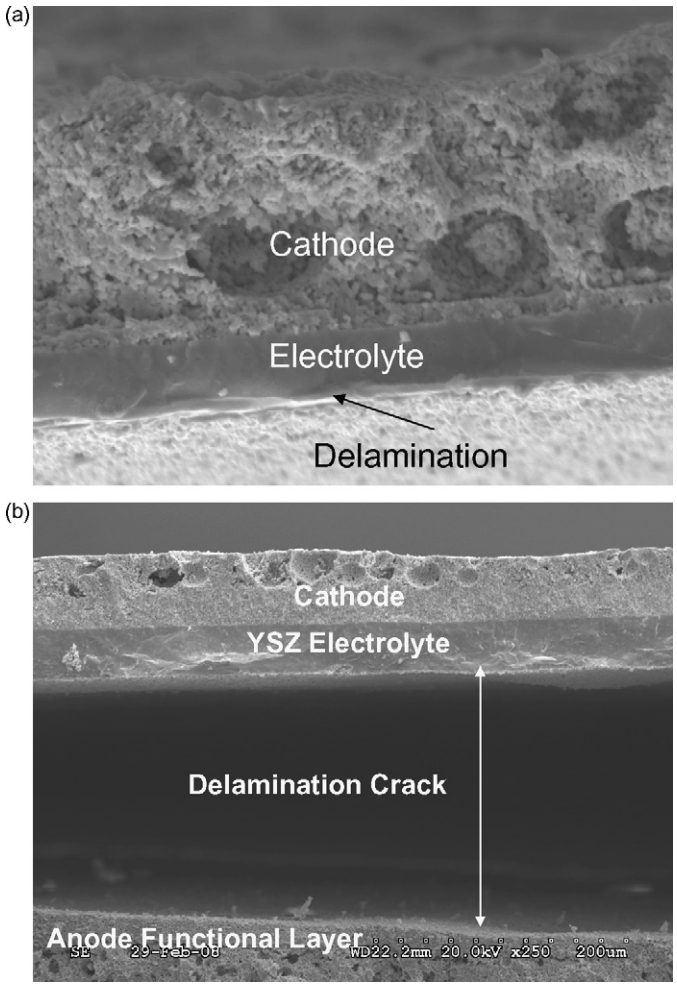

Fig. 11. (a) An SEM micrograph of a fully delaminated cell showing that delamination occurs along the electrolyte/anode interface with the cathode well bonded to the electrolyte. (b) An SEM micrograph of another partially delaminated cell showing that delamination occurs along the electrolyte/anode interface with the cathode well bonded to the electrolyte.

under a negative voltage causing delamination. In ref. [15], case corresponding to a high pressure buildup in the electrolyte just under cathode/electrolyte interface was examined. As described in refs. [15,21], relative transport properties of interfaces and electrolyte dictate the variation of μ_{O_2} through the electrolyte. The observation of delamination at the anode/electrolyte is consistent with

$$\mu^{c'}_{O_2} \approx \mu^{I}_{O_2} - 4er^{c'}_{i}\left|I'_{i}\right| \approx \mu^{I}_{O_2} - 4er^{c'}_{i}\left|I_{L}\right| < \mu^{I}_{O_2} \quad (10)$$

and

$$\mu^{a'}_{O_2} \approx \mu^{II}_{O_2} + 4er^{a'}_{i}\left|I'_{i}\right| \approx \mu^{II}_{O_2} + 4er^{a'}_{i}\left|I_{L}\right| > \mu^{II}_{O_2} > \mu^{c}_{O_2} \quad (11)$$

No data are available on various transport parameters ($r^{c'}_{i}$, $r^{c'}_{e}$, $r^{el'}_{i}$, $r^{el'}_{e}$, $r^{a'}_{i}$, $r^{a'}_{e}$), and thus the μ_{O_2} profile through the YSZ electrolyte at the present cannot be determined with certainty.

3.3. Development and measurement of high internal p_{O_2} in a bi-layer cell

An experiment with embedded electrode was conducted to verify the formation of high p_{O_2} under electrolytic conditions. Fig. 6 shows a schematic of a bi-layer sample YSZ/YSZ + 5% CeO_2 (added to increase electronic conductivity). Fig. 12 shows the measured voltage between the reference electrode on the YSZ surface, and

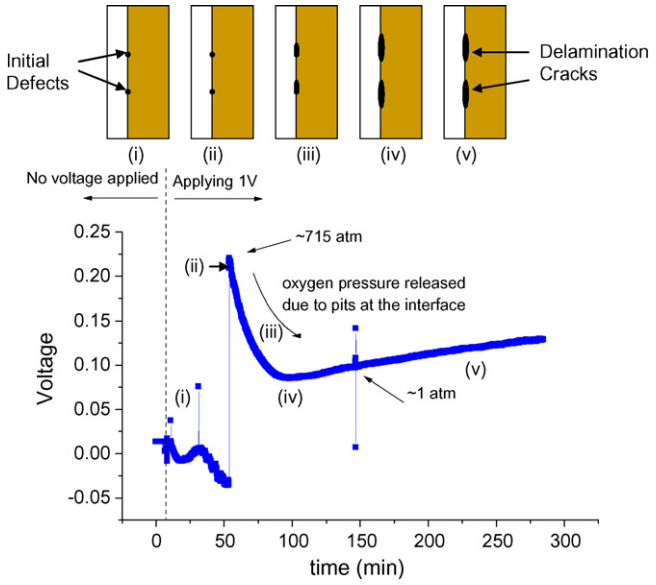

Fig. 12. Voltage measured between the embedded reference electrode at the YSZ/YSZ + ceria interface and the one on the YSZ surface with DC voltage (1 V) applied. The maximum estimated interface p_{O_2} was ~715 atm. Subsequent decrease in the measured voltage between the reference electrodes signifies interface cracking thereby releasing the pressure.

the embedded electrode, namely $\varphi_E - \varphi_S$. Before applying 1 V DC, the $\varphi_E - \varphi_S$ was ~0 V, consistent with p_{O_2} at the interface about the same as in the ambient atmosphere. Once 1 V DC was applied, after ~55 min, the $\varphi_E - \varphi_S$ increased sharply, reaching a value of ~0.22 V. Rapid increase in voltage implies that volume pressurized at the interface is quite small, as the time constant for pressurization is a monotonic function of volume [19,20]. This represents pressurization of small interface defects, labels (i) and (ii) in Fig. 12. The sharp rise in $\varphi_E - \varphi_S$ was followed by a slow drop to ~0.08 V in ~35 min (total ~90 min from start of experiment), and then continued to increase for additional 3 h. The slow drop in $\varphi_E - \varphi_S$ denotes slow growth of interface cracks/voids (labels (iii) and (iv) in Fig. 12). The slow increase in $\varphi_E - \varphi_S$ after ~100 min is consistent with a partially delaminated interface and a higher pressurization volume, label (v) in Fig. 12. Thereafter, the applied voltage was removed and the test was terminated. If the test had been continued, cracking along the interface is expected, as discussed in ref. [20].

Assuming electrode polarization is small compared to the ohmic loss, most of the applied 1 V DC drops across the sample as ohmic loss. Ionic conductivities of YSZ and YSZ + 5% CeO_2 are about the same. Thus, 50/1550 or ~0.032 V drops across the YSZ layer. If p_{O_2} at the interface were the same as in the atmosphere, $\varphi_E - \varphi_S$ would have been ~0.032 V. The maximum measured $\varphi_E - \varphi_S \approx 0.22$ V. This means there is an internal EMF due to a different p_{O_2} at the interface [21]. The corresponding EMF E, is given by $E \approx 0.22 - 0.032 = 0.188$ V. Thus, the p_{O_2} at the interface is given by

$$p^{int}_{O_2} = p^{amb}_{O_2} \exp\left(\frac{4eE}{k_B T}\right) = 0.21 \exp\left(\frac{4 \times 0.188 \times 1.6 \times 10^{-19}}{1.38 \times 10^{-23} \times 1073}\right)$$
$$\approx 715\ \text{atm} \approx 10,000\ \text{psi} \quad (12)$$

This calculation shows that a very large p_{O_2} develops at the interface. Decrease in $\varphi_E - \varphi_S$ thereafter reflects release of pressure as cracks develop at the interface (labels (ii), (iii) and (iv) in Fig. 12). As discussed in ref. [20], while high pressure develops, cracking

occurs in a slow and a stable manner[7]. At the minimum point (~0.08 V), the $p_{O_2}^{int} \sim 1.65$ atm. At the end of experiment, $\varphi_E - \varphi_S$ was ~0.125 V, which corresponds to $p_{O_2}^{int} \sim 11.5$ atm (label (v)). The expectation is that additional cracking will occur when pressure builds to a value sufficient to again satisfy fracture mechanical criteria [20]. This experiment confirms the development of high internal pressures under imposed electrolytic conditions in solid electrolytes. The objective of this experiment was to demonstrate the formation of high internal p_{O_2} under imposed electrolytic conditions.

3.4. Analysis of internal pressure in an SOFC operating abnormally

In terms of Nernst voltage, E, cell voltage, V_C, and various ionic and electronic resistances, μ_{O_2}'s in the *electrolyte* just under the cathode and the anode, are given by ref. [15]

$$\mu_{O_2}^{c} = \mu_{O_2}^{I} + 4e\left\{\frac{r_i^c(V_C - E)}{R_i} - \frac{r_e^c V_C}{R_e}\right\} \quad (13)$$

$$\mu_{O_2}^{a} = \mu_{O_2}^{II} - 4e\left\{\frac{r_i^a(V_C - E)}{R_i} - \frac{r_e^a V_C}{R_e}\right\} \quad (14)$$

where

$$R_i = r_i^c + r_i^{el} + r_i^a \quad (15)$$

$$R_e = r_e^c + r_e^{el} + r_e^a \quad (16)$$

in which r_i^{el} and r_e^{el} are respectively electrolyte ionic and electronic area specific resistances.

Using Eq. (9), for a cell test under a DC bias Eqs. (13) and (14) can also be given in terms of the bias voltage E_b. In what follows we will describe μ_{O_2} in terms of cell voltage, V_C (Eqs. (13) and (14)). The difference $\mu_{O_2}^{a} - \mu_{O_2}^{c}$ is thus given by

$$\mu_{O_2}^{a} - \mu_{O_2}^{c} = \mu_{O_2}^{II} - \mu_{O_2}^{I} + 4e\left\{\frac{(r_i^c + r_i^a)(E - V_C)}{R_i} + \frac{(r_e^c + r_e^a)V_C}{R_e}\right\} \quad (17)$$

or

$$\mu_{O_2}^{a} - \mu_{O_2}^{c} = -4eE + 4e\left\{\frac{(r_i^c + r_i^a)(E - V_C)}{R_i} + \frac{(r_e^c + r_e^a)V_C}{R_e}\right\} \quad (18)$$

where we have written

$$\mu_{O_2}^{I} - \mu_{O_2}^{II} = 4eE \quad (19)$$

Now $(r_i^c + r_i^a)/R_i \le 1$ and $(r_e^c + r_e^a)/R_e \le 1$. If the cell is operating normally, $E \ge V_C \ge 0$

we have $4e\{((r_i^c + r_i^a)/R_i)(E - V_C) + ((r_e^c + r_e^a)/R_e)V_C\} \le 4eE$ and thus from Eq. (18), note that $\mu_{O_2}^{a} - \mu_{O_2}^{c} < 0$. It also follows that, $\mu_{O_2}^{II} < \mu_{O_2}^{a} < \mu_{O_2}^{c} < \mu_{O_2}^{I}$ [21].

When a cell is operating abnormally, $V_C < 0$ and Eq. (17) becomes[8]

$$\mu_{O_2}^{a'} - \mu_{O_2}^{c'} = \mu_{O_2}^{II} - \mu_{O_2}^{I} + 4e\left\{\frac{(r_i^{c'} + r_i^{a'})(|V_C| + E)}{R_i'} - \frac{(r_e^{c'} + r_e^{a'})|V_C|}{R_e'}\right\} \quad (20)$$

[7] The actual oxygen pressure at the interface can be high but the net amount of oxygen as a gas may be negligible. Also, cracking is slow and stable since the rate of pressure generation is a function of the current [20].

[8] 'Primes' are placed over the specific resistances (transport parameters) and chemical potentials to emphasize abnormal cell behavior.

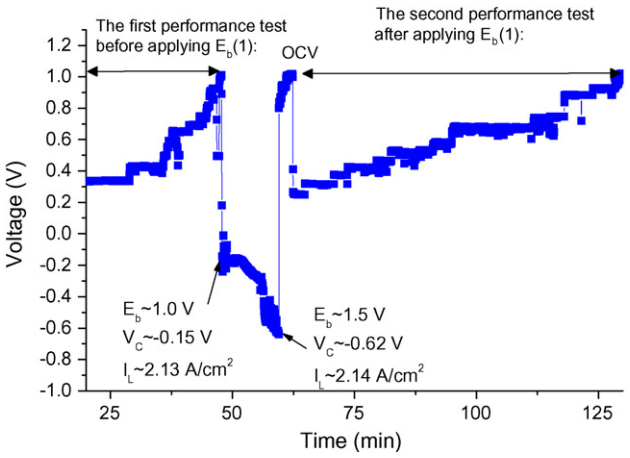

Fig. 13. Test on an another SOFC. The initial voltage vs. current density performance is given in the first part of the plot (~25 to ~50 min). The second part of the plot (~50 to ~60 min) shows test under an applied bias with cell operating under a negative voltage under a constant current (~2.13–2.14 A cm^{-2}). The last part of the plot (~62 to ~130 min) is cell performance measurement.

Now, relative values of $(r_i^{c'} + r_i^{a'})/R_i'$ and $(r_e^{c'} + r_e^{a'})/R_e'$ determine the sign of $\mu_{O_2}^{a'} - \mu_{O_2}^{c'}$. If $(r_i^{c'} + r_i^{a'})(|V_C| + E)/R_i' > (r_e^{c'} + r_e^{a'})|V_C|/R_e'$, note that the term in {} in Eq. (20) is positive. In the extreme case, if $(r_e^{c'} + r_e^{a'})/R_e' \approx 0$ (easy electron transfer across interfaces) but $(r_i^{c'} + r_i^{a'})/R_i' \approx 1$ (difficult ion transfer across interfaces), we have

$$\mu_{O_2}^{a'} - \mu_{O_2}^{c'} \approx \mu_{O_2}^{II} - \mu_{O_2}^{I} + 4e(|V_C| + E) \quad (21)$$

Using (19), Eq. (21) reduces to

$$\mu_{O_2}^{a'} - \mu_{O_2}^{c'} \approx 4e|V_C| > 0 \quad (22)$$

That is, $\mu_{O_2}^{a'} > \mu_{O_2}^{c'}$, and depending upon the magnitude of cell voltage (with $V_C < 0$), high pressures can develop just under anode/electrolyte interface (into the electrolyte) leading to delamination along (close to) electrolyte/anode interface.[9] This in fact is the case observed in the present work.

The observation that cell delaminates at the anode/electrolyte interface when operated under a negative voltage (Fig. 11) is consistent with Eq. (21), which is consistent with high ionic area specific resistances across electrode/electrolyte interfaces. It is understood that many different scenarios are possible depending upon relative values of ionic and electronic transport parameters as described in ref. [21]. Yet, all scenarios are based on a cell in a stack behaving abnormally.

3.5. Progress of interface delamination in a cell subjected to repeated operation under a negative cell voltage

Fig. 13 shows the results of a test on a cell subjected to alternate measurement of cell characteristics followed by alternate operation under a negative voltage. Fig. 13 shows the V_C during initial performance test (from ~25 to ~50 min). The V_C was varied between ~0.35 V and the OCV (~1.05 V). The corresponding voltage vs. current density plot is given in Fig. 14 (trace a – cell ASR ~0.35 Ω cm^2). A DC bias, E_b, of ~1.0 V was then applied to induce

[9] The case considered in ref. [15] was corresponding to difficult electron transfer and easy oxygen ion transfer across interfaces, in which case high pressure develops in the electrolyte just under the cathode – leading to cathode delamination.

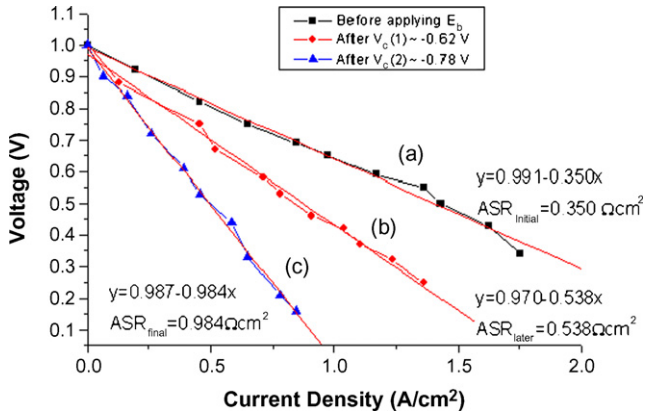

Fig. 14. Voltage vs. current density plots corresponding to: (a) initial test (prior to applying a DC bias) (ASR ~0.35 Ωcm^2), (b) after first operation under a DC bias (ASR ~0.538 Ωcm^2), (c) after the second test under a DC bias (ASR ~0.984 Ωcm^2). Increase in ASR when operated under DC bias is due to delamination.

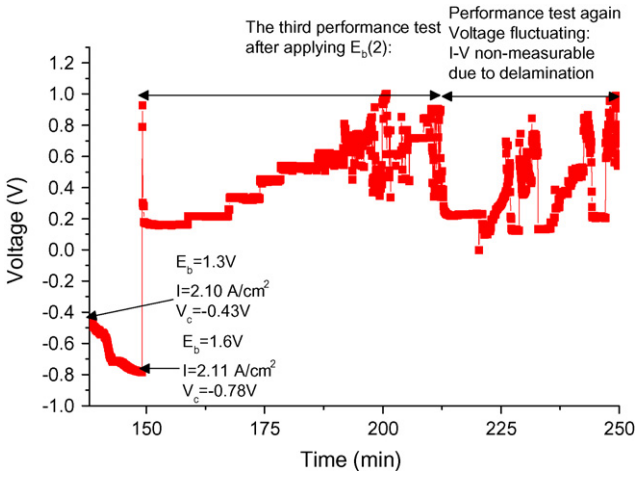

Fig. 15. Test on the same cell as in Fig. 13. The initial part (up to ~150 min) shows test under the second application of DC bias and operation under a negative cell voltage at constant current (2.11 A cm^{-2}). The cell voltage varied between −0.43 V and −0.78 V. The second part (~150 to ~200 min) of the figure shows the results of cell performance test (ASR ~0.984 Ωcm^2). Voltage vs. current density plot is given in Fig. 14 (trace c).

abnormal behavior. The corresponding V_C ~ −0.15 V and the current density ~2.13 A cm^{-2}. The test was conducted at a constant current for ~10 min over which the E_b automatically increased to ~1.5 V as cell degraded (decrease of V_C – increase in magnitude). The bias was then removed. The OCV immediately after was ~0.8 V, which gradually increased to ~1.05 V (Fig. 13). Another cell test was performed as shown in Fig. 13 with V_C varied between ~0.28 V and OCV (from ~62 to ~130 min). The voltage vs. current density plot is given in Fig. 14 (trace b – ASR ~0.538 Ωcm^2 which is considerably greater than in the initial test (ASR ~0.35 Ωcm^2)).

Finally, another test under a negative cell voltage was conducted. An E_b ~1.3 V was applied. The corresponding V_C ~ −0.43 V and the current density ~2.1 A cm^{-2}. The test was conducted for 10 min under a constant current over which the V_C decreased to ~−0.78 V (Fig. 15). The external bias was removed and a performance test was conducted (Fig. 14 – trace c, ASR ~0.984 Ωcm^2). Towards the end of test, OCV began to fluctuate (Fig. 15). The fluctuations are consistent with the occurrence of substantial delamination.

3.6. Analysis of delamination

Fig. 16(a) shows the variation of μ_{O_2} though the electrolyte in a cell behaving abnormally [15,21]. The maximum μ_{O_2} occurs in the electrolyte just under the anode/electrolyte interface. The corresponding p_{O_2} may be quite high – may be several atmospheres. Just outside the electrolyte, into the porous anode, the total pressure (fuel) is ~ 1 atm. That is, there is an abrupt change in pressure at the interface. Any defects such as small pores, grain boundaries, will develop large pressure (p_{O_2}) and delamination will begin.

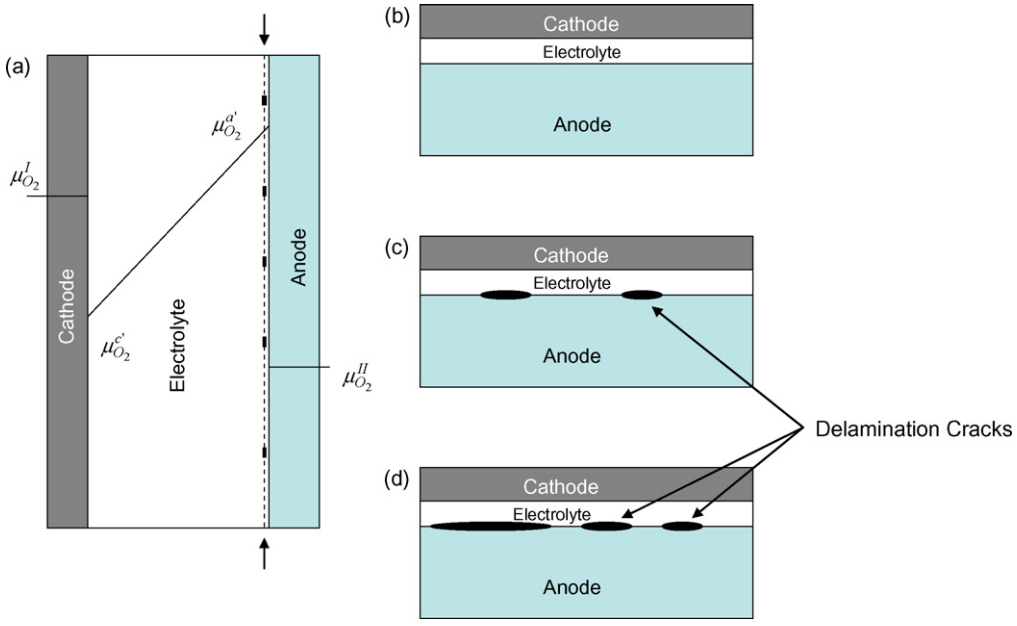

Fig. 16. (a) A schematic showing the variation of μ_{O_2} through a cell behaving abnormally. Delamination initiates within the electrolyte, very close to the anode/electrolyte interface, and then links up with the interface resulting in delamination along the interface. (b) A schematic showing the original cell, prior to subjecting to a negative voltage. (c) A schematic showing the formation of delamination cracks along the electrolyte/anode interface after subjecting the cell to negative voltage. (d) A schematic showing growth and coalescence of delamination cracks along the electrolyte/anode interface with further accumulation of damage.

The formed cracks will easily link up with the anode/electrolyte interface effectively reflecting the delamination as being along the anode/electrolyte interface, even when its initiation is just inside the electrolyte. In the following discussion, the delamination will be referred to as being occurring along the anode/electrolyte interface while still recognizing that its origin is just inside the electrolyte.

The initial ASR of the cell was $R_C^o \approx 0.35\ \Omega\text{cm}^2$. Fig. 16(b) shows a schematic of the cell prior to testing under a negative cell voltage. Delamination along (close to) an interface should reflect as increase in ASR with the ASR being inversely proportional to the area fraction of non-delaminated portion of the interface. If the delaminated area fraction is A_{del}, the corresponding cell ASR is given by

$$R_C = \frac{R_C^o}{(1 - A_{del})} \tag{23}$$

or

$$A_{del} = 1 - \frac{R_C^o}{R_C} \tag{24}$$

After the first test under a DC bias, the $R_C \sim 0.538\ \Omega\text{cm}^2$. The corresponding $A_{del} \approx 1 - (0.35/0.538) \approx 0.35$; that is ~35% of interface had delaminated. Fig. 16(c) shows a schematic with delamination along anode/electrolyte interface (in principle in the electrolyte just under the interface). Delamination may originate at a number of places. At the end of second test, the R_C ~0.984 Ωcm^2, with the corresponding $A_{del} \approx 1 - (0.35/0.984) \approx 0.64$ or ~64% of the interface had delaminated. Fig. 16(d) shows a schematic of this situation. After the second test, interface was almost completely delaminated (and consistent with unstable voltage in Fig. 15 beyond ~200 min). Fig. 11 shows SEM images of typical delaminated cells. Indeed, extensive delamination is apparent. An important point is that the total duration over which the cell was operated under a negative voltage was only about 20 min. These results thus suggest that in a real stack, once conditions leading up to abnormal behavior set in, subsequent degradation may occur within minutes, in accord with the analysis given in ref. [15]. It was observed that damage continued to grow even when the bias was removed, indicating that cracks continue to grow under the internal pressure built up. Many mechanisms of slow (sub critical) crack growth in ceramics are well known and continued damage during idling is expected, as observed. This explains the observed lower (larger in magnitude but negative in sign) cell voltage at the beginning of second test (Fig. 10) than the end voltage of the first test (Fig. 9).

3.7. Implications concerning SOFC stack life

The present work shows that once a cell begins to operate abnormally (under a negative voltage), degradation may be very rapid. Thus, stack life in situations where cell imbalance occurs is the time required for establishing conditions leading up to cell imbalance.

4. Summary

Using conventional alkaline cells, a battery with eight D cells and one AAA cell connected in series was tested. It was demonstrated that the AAA cell could be operated under a negative voltage due to cell imbalance. Once operation under a negative voltage commenced, the AAA cell began to rapidly degrade as reflected in rapid drop in voltage. The objective of this test was to demonstrate cell degradation due to cell imbalance in batteries. In order to electrochemically generate and measure high internal oxygen pressure in solid electrolytes, a bi-layer cell of YSZ/YSZ + ceria was made and tested under an applied 1 V DC. An embedded reference electrode was positioned at the interface. From the measured voltage across reference electrodes, it was estimated that a p_{O_2} as high as ~715 atm could be generated before the onset of cracking. These two experiments established the basis for the subsequent work on SOFC stack degradation. The main objective of this work was to explore solid oxide fuel cell stack degradation due to cell imbalance. Anode-supported solid oxide fuel cells were tested at 800 °C with H_2 as fuel and air as oxidant. In order to simulate 'bad' cell behavior (the one with higher resistance and operating under a negative voltage), a DC bias was applied to force the cell to operate under a negative voltage. As soon as the cell began to operate under a negative voltage, it began to degrade which reflected as decreasing cell voltage (increasing magnitude). Subsequent post test examination showed that delamination occurred along (in the electrolyte – close to the interface) the electrolyte/anode interface. The origin of delamination is related to the development of high internal p_{O_2} into the electrolyte, just under the electrolyte/anode interface. This work shows that SOFC stack degradation will likely occur if cell imbalance occurs. The propensity to stack degradation is expected to increase with increasing number of cells in a stack. Also, once a cell becomes bad, subsequent degradation may be very rapid – perhaps within a matter of minutes.

Acknowledgement

This work was funded by the U.S. Department of Energy under Grant Number DE-FG02-06ER46086.

References

[1] J.B. Olson, E.D. Sexton, Fourteenth Annual Battery Conference on Applications and Advances, IEEE (1999), pp. 155–159.
[2] E.D. Sexton, J.B. Olson, Fourteenth Annual Battery Conference on Applications and Advances, IEEE, (1999), pp. 25–29.
[3] J.B. Olson, E.D. Sexton, Fifteenth Annual Battery Conference on Applications and Advances, IEEE, (2000), pp. 205–210.
[4] P.T. Krein, R.S. Balog, Twenty-fourth Annual International Telecommunications Energy Conference, IEEE (2002), pp. 516–523.
[5] A. Lohmer, E. Karden, R.W. DeDoncker, Nineteenth Annual International Telecommunications Energy Conference, IEEE (1997), pp. 407–411.
[6] S. West, P.T. Krein, Twenty-second Annual International Telecommunications Energy Conference, IEEE (2000), pp. 439–446.
[7] T.T. Sack, J.C. Tice, R. Reynolds, Sixteenth Annual Battery Conference on Applications and Advances, IEEE (2001), pp. 157–159.
[8] N.H. Kutkut, H.L.N. Wiegman, D.M. Divan, D.W. Novotny, Tenth Annual Applied Power Electronics Conference, IEEE (1995), pp. 96–103.
[9] N.H. Kutkut, D.M. Divan, D.W. Novotny, Twelfth Industry Applications Society Annual Meeting, IEEE (1994), pp. 1008–1015.
[10] D. Berndt, U. Teutsch, J. Electrochem. Soc. 143 (3) (1996) 790–798.
[11] S. Atlung, B. Zachau-Christiansen, J. Power Sources 52 (1994) 201.
[12] M. Tang, T. Stuart, IEEE Trans. Ind. Electron. 40 (1) (2000) 201–211.
[13] S.T. Hung, D.C. Hopkins, C.R. Mosling, IEEE Trans. Ind. Electron. 40 (1) (2000) 96–104.
[14] P.T. Krein, S. West, C. Papenfuss, Sixteenth Annual Battery Conference on Applications and Advances, 2001, pp. 125–130.
[15] A. Virkar, J. Power Sources 172 (2007) 713–724.
[16] D. Kondepudi, I. Prigogine, Modern Thermodynamics: From Heat Engines to Dissipative Structures, John Wiley, New York, 1998.
[17] L. Heyne, Mass Transport in Oxides, 296, NBS Special Publication, 1968, pp. 149–164.
[18] C. Wagner, Proceedings of the 7th meeting on International Committee On Electrochemistry, Thermodynamics and Kinetics, Lindau, Butterworth (1957), pp. 361–377.
[19] A.V. Virkar, J. Mater. Sci. 20 (1985) 552.
[20] A.V. Virkar, J. Nachlas, A.V. Joshi, J. Diamond, J. Am. Ceram. Soc. 73 (11) (1990) 3382.
[21] A.V. Virkar, J. Power Sources 147 (2005) 8.
[22] H.-T. Lim, A.V. Virkar, J. Power Sources 180 (2008) 92–102.